

Spontaneous symmetry breaking in continuous waves, dark solitons, and vortices in linearly coupled bimodal systems

Hidetsugu Sakaguchi¹ and Boris A. Malomed^{2,3}

¹*Department of Applied Science for Electronics and Materials,
Interdisciplinary Graduate School of Engineering Sciences,
Kyushu University, Kasuga, Fukuoka 816-8580, Japan*

²*Department of Physical Electronics, School of Electrical Engineering,
Faculty of Engineering, and Center for Light-Matter Interaction,
Tel Aviv University, P.O. Box 39040 Tel Aviv, Israel and*

³*Instituto de Alta Investigación, Universidad de Tarapacá, Casilla 7D, Arica, Chile*

We introduce a model governing the copropagation of two components which represent circular polarizations of light in the optical fiber with relative strength $g = 2$ of the nonlinear repulsion between the components, and linear coupling between them. A more general system of coupled Gross-Pitaevskii (GP) equations, with $g \neq 2$ and the linear mixing between the components, is considered too. The latter system is introduced in its one- and two-dimensional (1D and 2D) forms. A new finding is the spontaneous symmetry breaking (SSB) of bimodal CW (continuous-wave) states in the case of $g > 1$ (in the absence of the linear coupling, it corresponds to the immiscibility of the nonlinearly interacting components). The SSB is represented by an exact asymmetric CW solution. An exact solution is also found, in the case of $g = 3$, for stable dark solitons (DSs) supported by the asymmetric CW background. For $g \neq 3$, numerical solutions are produced for stable DSs supported by the same background. Moreover, we identify a parameter domain where the fully miscible (symmetric) CW background maintains stable DSs with the *inner SSB* (separation between the components) in its core. In 2D, the GP system produces stable vortex states with a shift between the components and broken isotropy. The vortices include ones with the inter-component shift imposed by the asymmetric CW background, and states supported by the symmetric background, in which the intrinsic shift (splitting) is exhibited by vortical cores of the two components.

I. INTRODUCTION AND THE MODEL

Spontaneous symmetry breaking (SSB) is a ubiquitous feature of phenomenology which occurs in a great variety of nonlinear systems. Various manifestations of SSB have been studied in detail, theoretically and experimentally, in nonlinear optics and photonics and in atomic BECs (Bose-Einstein condensates) [1]. A basic setting for the realization of SSB is provided by linearly coupled dual-core (two-component) systems with intrinsic (intra-core) nonlinearity, such as twin-core optical fibers (a.k.a. nonlinear couplers) [2, 3], tunnel-coupled traps for matter waves [4–6], microwave resonators [7], and some other physical systems. In these systems, SSB is initiated by instability of symmetric two-component states against small perturbations which break their symmetry. In their simplest form, the corresponding SSB effects occur in the continuous-wave (CW) settings [8]. However, CW states are subject to the modulational instability (MI) in the case of the self-focusing intra-core nonlinearity, which tends to split them into chains of bright solitons [9]. Thus, much interest has been drawn to the realization of SSB in two-component solitons carried by dual-core optical fibers [10]–[22], see also review [24]. The conservative dual-core systems are modeled by systems of two linearly-coupled nonlinear Schrödinger (NLS) equations, while their dissipative counterparts are represented by systems of coupled complex Ginzburg-Landau equations, which predict SSB in two-component dissipative solitons [25, 26].

The natural sign of the intrinsic nonlinearity in BEC is self-repulsive [27], which is possible too in defocusing nonlinear optical media [28, 29]. Intrinsic instabilities take place in two-component self-defocusing system if coefficients $g_{11,22}$ and $g_{12} \equiv g_{21}$ of the cross- and self-repulsion of the components satisfy the basic immiscibility condition [30], $g_{12} > \sqrt{g_{11}g_{22}}$. Below, we consider the system with $g_{11} = g_{22}$, and define the relative strength of the cross-repulsion as $g \equiv g_{12}/g_{11,22}$, in terms of which the immiscibility condition amounts to $g > 1$. In this case, spatially or temporally periodic perturbations give rise to a specific form of MI, which breaks the uniform CW state into a chain domain walls (DWs) separating domains populated by the different immiscible components [31].

The SSB phenomenology in linearly-coupled dual-core systems with intrinsic defocusing nonlinearities was predicted in two-component gap solitons, that are supported by such systems if both cores carry a spatially-periodic potential [5], which is necessary to create gaps solitons as a result of the interplay of this potential with the self-repulsion [32]. The SSB between linearly coupled components in 1D and 2D systems combining the self-defocusing and a trapping harmonic-oscillator potential was addressed in Ref. [22], which included the consideration of 2D vortex states with the broken symmetry. However, a possibility of SSB in two-component systems combining the linear coupling between the components with the self- and cross-repulsion in the free space has not been addressed previously. The objective

of the present work is to introduce such a physically relevant system, produce SSB states in it, including CWs, two-component one-dimensional (1D) dark solitons (DSs), and two-component 2D vortices, in analytical and numerical forms, and investigate the stability of these states.

The system is introduced in Section 2, in the form of the system of a linearly-coupled Gross-Pitaevskii (GP) equations for wave functions $\phi(x)$ and $\psi(x)$. General CW analytical solutions with the unbroken and broken symmetry, as well as specific exact DS solutions, are found in Section 3. The stable asymmetric CW states exist precisely in the case when the immiscibility condition $g > 1$ holds. Further, in the special case of $g = 3$, which implies strong immiscibility, we find an exact DS solution, which connects two asymmetric CW states with opposite overall signs at $x = \pm\infty$. While this DS is maintained by the asymmetric CW background, it keeps its intrinsic inversion symmetry, expressed by relation

$$\phi(-x) = -\psi(x). \quad (1)$$

For $g \neq 3$, we find more general exact DS asymmetric solutions pinned to the attractive or repulsive Pöschl-Teller (PT) potential, of the sech^2 type [23] (although, unlike the exact DS solutions found at $g = 3$, they are unstable). Section 3 also reports the MI analysis for the CW symmetric states at the SSB threshold, which demonstrates that they are stable, hence the asymmetric CW states, produced by the SSB bifurcation, inherit the modulational stability from the symmetric ones.

Systematically produced numerical results are reported in Section 4, for both the symmetry-breaking DSs and their 2D counterparts, which, as it may be naturally expected [28], are two-component vortices. The 1D numerical solutions are produced for a pair of DSs which are placed at opposite positions in a domain of a large size, subject to periodic boundary conditions, with the aim to preclude artifacts that may be induced by boundary conditions. In particular, stable numerical solutions are produced for the symmetry-breaking DSs in the general case, $g \neq 3$. A noteworthy finding, revealed by the numerical solution and explained by a variational approximation (VA), is that immiscibility (actually, a shift between the components) may take place in the core of the 1D DSs or 2D vortices, even in the case when the CW background which supports them remains fully miscible (symmetric). We categorize this case as “inner” immiscibility, to distinguish it from the “outer” immiscibility, featured by the external CW background (which implies the occurrence of immiscibility in the core region as well). The paper is concluded by Section 5.

II. THE MODEL

In the scaled form, the 1D system of linearly coupled GP equations for mean-wave functions ϕ and ψ of the two components of the binary BEC, with the repulsive self- and cross-interactions, is

$$i\phi_t = -\kappa\psi - \frac{1}{2}\phi_{xx} + (|\phi|^2 + g|\psi|^2)\phi, \quad (2)$$

$$i\psi_t = -\kappa\phi - \frac{1}{2}\psi_{xx} + (|\psi|^2 + g|\phi|^2)\psi, \quad (3)$$

where t is time, x the spatial coordinate, g the above-mentioned relative strength of the cross-repulsion, and κ , which is defined to be positive, is the coefficient of the linear mixing between components ϕ and ψ . If ϕ and ψ represent two different hyperfine states of the same atom, the linear mixing is induced by a resonant electromagnetic (radiofrequency) field [33, 34].

The same system of Eqs. (2) and (3), with $g = 2$, time t replaced by the propagation distance, z , and coordinate x replaced by the reduced time, $\tau = t - z/V_{\text{gr}}$, is the pair of coupled NLS equations governing the copropagation of two circular polarizations of light, with group velocity V_{gr} of the carrier wave, in an optical fiber with the self-defocusing cubic nonlinearity [9]. In that case, the linear mixing is induced by an elliptic deformation of the originally circular fiber’s core (in other words, by the birefringence of the linearly polarized modes).

Stationary solutions to Eqs. (2) and (3) with chemical potential $-k$ (or propagation constant k , in the case of the optical-fiber model) are looked for as

$$\phi(x, t) = e^{ikt}u(x), \quad \psi(x, t) = e^{ikt}v(x). \quad (4)$$

The substitution of expressions (4) in Eqs. (2) and (3) yields equations

$$-ku + \kappa v = -\frac{1}{2}\frac{d^2u}{dx^2} + u^3 + gv^2u, \quad (5)$$

$$-kv + \kappa u = -\frac{1}{2}\frac{d^2v}{dx^2} + v^3 + gu^2v. \quad (6)$$

for real functions $u(x)$ and $v(x)$.

The norm of the stationary solution (4), which determines the total number of atoms in the binary BEC, or the total beam power in the case of the optical realization of Eqs. (2) and (3), is

$$N = \int_{-\infty}^{+\infty} n(x)dx, \quad n(x) = |u(x)|^2 + |v(x)|^2. \quad (7)$$

Similarly, the Hamiltonian of the coupled system (2), (3), corresponding to the same stationary solution, is

$$H = \int_{-\infty}^{+\infty} h(x)dx, \quad (8)$$

with the Hamiltonian density

$$h = \frac{1}{2} \left[\left(\frac{du}{dx} \right)^2 + \left(\frac{dv}{dx} \right)^2 \right] + \frac{1}{2} (u^4 + v^4) + gu^2v^2 - 2\kappa uv. \quad (9)$$

In particular, the above-mentioned immiscibility condition $g > 1$ (in the case of $\kappa = 0$) [30] immediately follows from Eq. (9), comparing the mixed and demixed states that occupy a large domain of size L . For the former state, with densities $u^2 = v^2 \equiv n/2$, which are uniformly distributed in the entire domain, and for the latter state, which has densities $(u^2 = n, v^2 = 0)$ and $(u^2 = 0, v^2 = n)$ in two halves of the domain, separated by the DW, so that both states share the same total norm, $N = nL$, the values of the energy (Hamiltonian), as produced by Eqs. (8) and (9), are

$$E_{\text{mixed}} = (g + 1) Ln^2/4, \quad E_{\text{demixed}} = Ln^2/2 \quad (10)$$

(where the DW energy, which does not grow with the increase of L , is neglected). The comparison of the energies immediately demonstrates $E_{\text{demixed}} < E_{\text{mixed}}$ at $g > 1$, i.e., the immiscible state provides the energy minimum in this case.

III. EXACT ANALYTICAL RESULTS

A. SSB (spontaneous symmetry breaking) of CW states

For CW (x -independent) states, the derivatives in Eqs. (5) and (6) are dropped, reducing them to a linearly coupled system of cubic equations:

$$-ku + \kappa v = u^3 + gv^2u, \quad (11)$$

$$-kv + \kappa u = v^3 + gu^2v. \quad (12)$$

A straightforward solution of the coupled equations (11) and (12) yields the symmetric state,

$$u_s = v_s = \sqrt{\frac{\kappa - k}{g + 1}}, \quad (13)$$

with density

$$n_s = u_s^2 + v_s^2 = 2 \frac{\kappa - k}{g + 1}. \quad (14)$$

and the antisymmetric state,

$$u_{\text{anti}} = -v_{\text{anti}} = \sqrt{\frac{-k - \kappa}{g + 1}}. \quad (15)$$

These states exist in the regions of the chemical potential

$$\text{symm} : k < \kappa; \quad \text{antisymm} : k < -\kappa \quad (16)$$

(recall $\kappa > 0$ is fixed by definition; in the absence of the linear coupling, i.e., $\kappa = 0$, Eq. (16) reduces to $k < 0$). In fact, the antisymmetric state is not relevant, because the corresponding linear-coupling term $-2\kappa uv$ in the Hamiltonian density (9) is positive, unlike the negative one corresponding to the symmetric state, hence the antisymmetric state tends to be unstable, as it cannot realize the energy minimum.

SSB is represented by the exact asymmetric solution of the coupled equations (11) and (12), which is obtained replacing the equations by their sum and difference, and factorizing the resultant equations:

$$\{u_{\text{as}}^2, v_{\text{as}}^2\} = -\frac{k}{2} \pm \sqrt{\frac{k^2}{4} - \frac{\kappa^2}{(g-1)^2}}. \quad (17)$$

The relative sign of the components of this solution is determined by the relation

$$u_{\text{as}}v_{\text{as}} = \frac{\kappa}{g-1} \quad (18)$$

(which is compatible with Eq. (17)), i.e., the signs of both components are identical in the case of interest, $g > 1$, where the immiscibility is possible. Thus, unlike the SSB effect, spontaneous breaking of the antisymmetry is not possible.

The asymmetric solution (17) exists, for given $\kappa > 0$, in the following region of the chemical potential ($-k$):

$$-k > -k_{\text{thr}} \equiv \frac{2\kappa}{g-1}, \quad (19)$$

cf. Eq. (16), or, in terms of the density,

$$n_{\text{as}} \equiv u_{\text{as}}^2 + v_{\text{as}}^2 = -k > n_{\text{thr}} \equiv \frac{2\kappa}{g-1}, \quad (20)$$

where k_{thr} is the value of $k < 0$ at which the square root vanishes in Eq. (17). With the increase of the density of the symmetric state [see Eq. (14)], the SSB bifurcation takes place at the threshold value (20), at which the symmetric solution (13) is

$$(u_s^2)_{\text{thr}} = (v_s^2)_{\text{thr}} = \frac{\kappa}{g-1}, \quad (21)$$

cf. Eq. (21).

It is natural to expect that the transition from the symmetric state to the asymmetric one leads to the decrease of the state's energy. Indeed, the substitution of the asymmetric solution (17), (18) in the Hamiltonian density (9) yields the following expression, as a function of the density:

$$h_{\text{as}} = \frac{n^2}{2} - \frac{\kappa^2}{g-1}. \quad (22)$$

On the other hand, the substitution of the symmetric CW state (13) in expression (9), taking into regard expression (14) for the respective density, yields

$$h_s = \frac{(g+1)}{4}n^2 - \kappa n. \quad (23)$$

Then, it follows from Eqs. (22) and (23) that, in the case of $n > n_{\text{thr}}$, when the symmetric and asymmetric CW states coexist for the same density, the difference between their energy densities is

$$h_s - h_{\text{as}} = \frac{g-1}{4}(n - n_{\text{thr}})^2 > 0. \quad (24)$$

Thus, the SSB transition from the symmetric state to the asymmetric one indeed leads to the decrease of the energy.

B. Modulational stability of the symmetric CW state at the SSB-bifurcation point

The CW states found above are physically relevant ones if they are not subject to MI. The modulational stability can be explored in an analytical form for the symmetric CW state, while the analysis is too cumbersome for the

asymmetric one. The most relevant result is the one for the symmetric CW at the SSB-bifurcation point (19), (21), as the verification of the modulational stability at this point implies that the asymmetric CW inherits the stability.

To perform the analysis, solutions to Eqs. (2) and (3) are looked for in the Madelung form:

$$\phi(x, t) = a(x, t) \exp(i\alpha(x, t)), \psi(x, t) = b(x, t) \exp(i\beta(x, t)), \quad (25)$$

where $a(x, t)$, $b(x, t)$ and $\alpha(x, t)$, $\beta(x, t)$ are real amplitudes and phases of wave functions ϕ and ψ . The substitution of expressions (25) leads to a system of four real equations:

$$a_t + \frac{1}{2}a\alpha_{xx} + a_x\alpha_x - \kappa b \sin = 0, \quad (26)$$

$$b_t + \frac{1}{2}b\beta_{xx} + b_x\beta_x + \kappa a \sin(\alpha - \beta) = 0, \quad (27)$$

$$-a\alpha_t + \frac{1}{2}a_{xx} - \frac{1}{2}a\alpha_x^2 + \kappa b \cos(\alpha - \beta) - a^3 - 2b^2a = 0, \quad (28)$$

$$-b\beta_t + \frac{1}{2}b_{xx} - \frac{1}{2}b\beta_x^2 + \kappa a \cos(\alpha - \beta) - b^3 - 2ab = 0. \quad (29)$$

According to Eqs. (19) and (21), the symmetric CW (13) at the bifurcation point corresponds to the solution of equations (26)-(29) in the form of $\alpha = \beta = -2\kappa(g-1)^{-1}t$, $a_s = b_s = \sqrt{\kappa/(g-1)}$. For the stability analysis, perturbed solutions are looked for as

$$\{a(x, t), b(x, t)\} = \sqrt{\kappa/(g-1)} + \{a_1, b_1\} \exp(\gamma t - iqx), \quad (30)$$

$$\{\alpha(x, t), \beta(x, t)\} = -2\kappa(g-1)^{-1}t + \{\alpha_1, \beta_1\} \exp(\gamma t - iqx), \quad (31)$$

where $a_1, b_1, \alpha_1, \beta_1$ are amplitudes of infinitesimal perturbations, γ is the instability growth rate, and q is an arbitrary real wavenumber of the perturbation. MI takes place if one has $\text{Re}(\gamma(q)) > 0$ at any real value of q .

The substitution of the perturbed solution (30), (31) in Eqs. (26)-(29) and linearization with respect to the infinitesimal perturbations leads to the dispersion equation, which determines γ as a function of q :

$$16(g-1)\gamma^4 + 8q^2 [4g\kappa + (g-1)q^2] \gamma^2 + q^4 [(g-1)q^4 + 8g\kappa q^2 + 16\kappa^2(g+1)] = 0. \quad (32)$$

All roots of the biquadratic equation (32) are pure imaginary ones:

$$\gamma_{1,2} = \pm iq \sqrt{\kappa + \frac{q^2}{4}}, \quad \gamma_{3,4} = \pm iq \sqrt{\kappa \frac{g+1}{g-1} + \frac{q^2}{4}}, \quad (33)$$

hence there is no MI at the SSB-bifurcation point.

C. The exact solution for the symmetry-breaking dark soliton (DS) in the case of $g = 3$

The symmetric and antisymmetric CW states, given by Eqs. (13) and (15), respectively, support symmetric and antisymmetric two-component DSs:

$$v_{\text{DS}}(x) = u_{\text{DS}}(x) = \sqrt{\frac{-k + \kappa}{g+1}} \tanh\left(\sqrt{\kappa - k}x\right); \quad (34)$$

$$v_{\text{DS}}(x) = -u_{\text{DS}}(x) = \sqrt{\frac{-k - \kappa}{g+1}} \tanh\left(\sqrt{-k - \kappa}x\right). \quad (35)$$

Note that the symmetric and antisymmetric DSs (34) and (35) are transformed into each other by the substitution,

$$u \rightarrow u, v \rightarrow -v, \kappa \rightarrow -\kappa, x \rightarrow -x, \quad (36)$$

with respect to which the systems of Eqs. (2), (3) and (5), (6) are invariant.

On the other hand, it has been known since long ago [35] that the system of coupled real NLS equations (5), (6) with the special value $g = 3$ of the inter-component interaction coefficient and no linear coupling ($\kappa = 0$) admits an exact DW solution. Then, the exact solution with $g = 3$ was extended to the system of Eqs. (5), (6) with $\kappa \neq 0$ [36]:

$$\begin{cases} u_{\text{DW}}(x) \\ v_{\text{DW}}(x) \end{cases} = \frac{1}{2} \begin{cases} \sqrt{-k + \kappa} + \sqrt{-k - \kappa} \tanh(\sqrt{-k - \kappa}x) \\ \sqrt{-k + \kappa} - \sqrt{-k - \kappa} \tanh(\sqrt{-k - \kappa}x) \end{cases}, \quad (37)$$

which satisfies the boundary conditions

$$u(x = +\infty) = v(x = -\infty) \equiv v_{\text{as}}(g = 3), v(x = +\infty) = u(x = -\infty) \equiv u_{\text{as}}(g = 3), \quad (38)$$

with $u_{\text{as}}(g = 3)$ and $v_{\text{as}}(g = 3)$ given by Eqs. (17) and (18) with $g = 3$. Thus, the DW state (37) separates two asymmetric CW states which are mirror images of each other.

A new result reported here is the following exact DS solution of the system of Eqs. (5) and (6), which is actually produced by the application of substitution (36) to the DW (37):

$$\begin{cases} u_{\text{DS}}(x) \\ v_{\text{DS}}(x) \end{cases} = \frac{1}{2} \begin{cases} \sqrt{-k - \kappa} + \sqrt{-k + \kappa} \tanh(\sqrt{-k + \kappa}x) \\ -\sqrt{-k - \kappa} + \sqrt{-k + \kappa} \tanh(\sqrt{-k + \kappa}x) \end{cases}, \quad (39)$$

which is subject to the boundary conditions

$$u(x = +\infty) = -v(x = -\infty) \equiv u_{\text{as}}(g = 3), v(x = +\infty) = -u(x = -\infty) \equiv v_{\text{as}}(g = 3), \quad (40)$$

cf. Eq. (38). The relation of the present DS solution to the background asymmetric CW states, fixed as per Eq. (40), implies that the DS is a result of the SSB occurring with the symmetric two-component DS (34). On the other hand, the DS solution (39), being subject to the boundary conditions (40), demonstrates its inversion symmetry, expressed by relation (1) [in other words, by its counterpart $v_{\text{DS}}(-x) = -u_{\text{DS}}(x)$].

Unlike the DW solution (37), which keeps positive values of both components at all x , the two components of DS (39) have zero-crossing [$u(x_{\text{ZC}}^{(u)}) = 0$, $v(x_{\text{ZC}}^{(v)}) = 0$] points, the presence of which is the hallmark of DS states. These points are determined by relations

$$\tanh(\sqrt{-k + \kappa}x_{\text{ZC}}^{(u,v)}) = (-, +) \sqrt{\frac{-k - \kappa}{-k + \kappa}}, \quad (41)$$

Both the DW and DS solutions (37) and (39) exist in the region of $k < -\kappa$, which coincides with the existence condition (19) for the asymmetric CW state (17), with $g = 3$.

D. The system with the Pöschl-Teller (PT) potential

To construct an exact DS solution with an asymmetric CW background at $g \neq 3$, one can add the PT potential to the underlying system of Eqs. (2)-(3):

$$i \frac{\partial \phi}{\partial t} = -\frac{1}{2} \frac{\partial^2 \phi}{\partial x^2} + (|\phi|^2 + g|\psi|^2) \phi + \frac{W}{\cosh^2(\alpha x)} \phi - \kappa \psi, \quad (42)$$

$$i \frac{\partial \psi}{\partial t} = -\frac{1}{2} \frac{\partial^2 \psi}{\partial x^2} + (|\psi|^2 + g|\phi|^2) \psi + \frac{W}{\cosh^2(\alpha x)} \psi - \kappa \phi, \quad (43)$$

with specially selected values of the potential's strength and width:

$$W = \frac{3 - g}{g - 1} \frac{g - 1 + 2\kappa}{4}, \quad \alpha = \sqrt{\frac{g - 1 + 2\kappa}{2}}. \quad (44)$$

This potential can be readily implemented in the experimental setting for BEC with the help of an appropriately shaped laser beam illuminating the condensate [37, 38]. Note that the PT potential is attractive or repulsive [with Eq. (44) yielding $W < 0$ or $W > 0$] in the case of $g > 3$ or $g < 3$, respectively.

The system of Eqs. (42) and (43) with the PT potential subject to conditions (44) admits the exact DS solution:

$$\begin{cases} \phi(x) \\ \psi(x) \end{cases} = \frac{1}{2} e^{-it} \begin{cases} A + B \tanh(\alpha x) \\ -A + B \tanh(\alpha x) \end{cases}, \quad (45)$$

with amplitudes

$$A = \sqrt{\frac{g-1-2\kappa}{g-1}}, \quad B = \sqrt{\frac{g-1+2\kappa}{g-1}}, \quad (46)$$

cf. the above solution (39). Factor e^{-it} in expression (45) implies that the chemical potential is here fixed as $-k = 1$ by means of scaling. It is easy to see that, with respect to the adopted scaling $k = -1$, the CW background maintaining the DS produced by expressions (45) and (46) is exactly given by Eq. (17). In particular, the present DS solution exists at $g-1 > 2\kappa$, which is exactly the same as condition (19) (with $k = -1$), under which the asymmetric CW solution (17) exists.

Due to the inequality $B > A$, following from Eq. (46), the DS solution (45) demonstrates that both DS components have zero-crossing points determined by relations

$$\tanh\left(\alpha x_{ZC}^{(\phi,\psi)}\right) = (-, +) \frac{A}{B}, \quad (47)$$

cf. Eq. (41). As well as the exact DS solution (39), the one given by Eqs. (45) and (46) is also subject to the inversion symmetry (1). However, unlike the stable DS (39), the one given by Eqs. (42)-(46) is unstable, as indicated below.

IV. NUMERICAL AND VARIATIONAL RESULTS FOR DSS (DARK SOLITONS) IN 1D AND VORTICES IN 2D

A. Symmetry-breaking 1D dark solitons: numerical results

While the SSB phenomenology for the CW solutions of the coupled GP equations (2) and (3) is fully described by the simple analytical solution provided by Eqs. (17) and (18), the solution for the DS supported by the asymmetric DW background is available in the analytical form, given by Eq. (39), only in the special case of $g = 3$ [and also, for $g \neq 3$, in the presence of the specially designed PT potential with parameters (44)]. In this subsection we aim to produce generic symmetry-breaking DS solutions, for $g \neq 3$, in the numerical form and verify their stability.

The stationary DS solutions were obtained by means of the imaginary-time propagation method [39, 40], while their stability was tested by simulations of the perturbed evolution in real time. The numerical solutions were actually constructed for a pair of DSs, placed at diametrically opposite positions in a domain of a large size L , subject to periodic boundary conditions, as this setting makes it possible to eliminate artifacts induced by boundary conditions of other types (Dirichlet's or Neumann's, fixed at edges of a non-circular solution domain).

In the case of the chemical potential $-k$ subject to condition (19), when the stable CW state is the asymmetric one (17), the numerically found stable symmetry-breaking DSs connect these states, satisfying the boundary conditions (40), with $g \neq 3$. An example is shown in Fig. 1(a), for

$$g = 1.2, \kappa = 0.06, k = -1.01 \quad (48)$$

[note that these values indeed satisfy condition (19)]. In this and all other plots for 1D DSs, the total norm of the solution, constructed on the circumference of perimeter $L = 100$, is $\int_{-L/2}^{+L/2} [|u(x)|^2 + |v(x)|^2] dx = 100$ [cf. definition (7) for the infinite domain]. A peculiarity of the exact DS solution (39), available at $g = 3$, is that the difference of its two components is a constant, which does not depend on coordinate x : $u_{DS}(x; g = 3) - v_{DS}(x; g = 3) = \sqrt{-k - \kappa}$ at any x . On the contrary, at $g \neq 3$ numerically found DS solitons have $u(x) - v(x)$ depending on x [in particular, this is the case for the DS shown in Fig. 1(a)].

A new finding produced by the numerical solutions is that symmetry-breaking DS solitons, with splitting between $u(x)$ and $v(x)$ (i.e., partial immiscibility of the two components) occurring in the core of the DS, exist as well in the case when condition (19) *does not hold*, i.e., the asymmetric CW states *do not exist* (in other words, the CW state remains *fully miscible*). An example of such a stable DS, supported by the symmetric CW background (13), with the partial immiscibility observed in the DS's core, is presented in Fig. 1(b), for parameters

$$g = 1.2, \kappa = 0.28, k = -0.859. \quad (49)$$

The above-mentioned *outer* and *inner* immiscibilities, i.e., the existence of the DS states supported by the asymmetric CW background, as determined by condition (19), and, on the other hand, the splitting of $u(x)$ and $v(x)$ in the core of the DS supported by the miscible (symmetric) CW background, are quantified in Fig. 1(c) by the

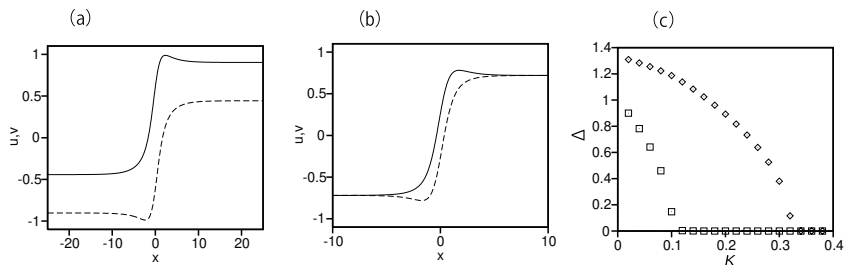


FIG. 1. (a) and (b): Profiles of components $u(x)$ and $v(x)$ in the numerically constructed stable symmetry-breaking DSs which connect, respectively, the partly immiscible or fully miscible CW states at $x = \pm\infty$. The corresponding parameters are given by Eq. (48) for (a) and (49) for (b). In both cases, the total norm is $N = 100$, and the solutions are constructed, as DS pairs, on the circumference of perimeter $L = 100$ (here, only one DS is displayed, in the interval of $-L/4 < x < +L/4$). (c) The outer and inner immiscibilities in the DSs, with fixed $N = 100$, $L = 100$, and $g = 1.2$, are characterized by dependences of $\Delta \equiv |u(x) - v(x)|$ on the linear coupling κ at $x = -L/4$ (squares) and $x = 0$ (rhombuses).

respective splittings, i.e., $\Delta \equiv |u(x) - v(x)|$ at $x = L/4$ (far from the DS core) and at $x = 0$ (at the DS center), plotted vs. the linear-coupling constant κ . It is seen that the outer immiscibility occurs at $\kappa < 0.11$ [in agreement with condition (19)], while the inner immiscibility persists at essentially larger values of the coupling, *viz.*, at $\kappa < 0.33$. The latter effect is qualitatively explained by the fact that the opposite signs of $u(x)$ and $v(x)$ in the DS core make the corresponding linear-mixing term $-2\kappa uv$ in the energy density (9) positive, which is an obstacle for mixing, unlike the negative mixing term in the energy density for the CW state. Below, a more accurate explanation of the inner immiscibility in the case of the symmetric CW background is proposed, based on VA.

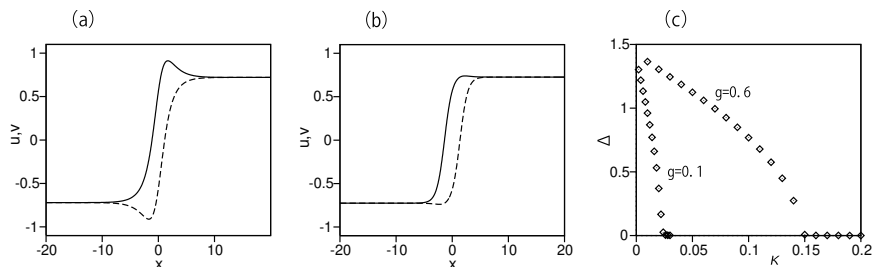


FIG. 2. (a) and (b): The same as in Fig. 1(b), but for $g = 1.0$, $\kappa = 0.1$, $k = -0.925$, and $g = 0.1$, $\kappa = 0.006$, $k = -0.573$. (c) The measure of the core's immiscibility, $\Delta \equiv |u(x = 0) - v(x = 0)|$, for the DSs with the inner shift between the components, vs. the linear coupling, κ , at $g = 0.1$ and 0.6 .

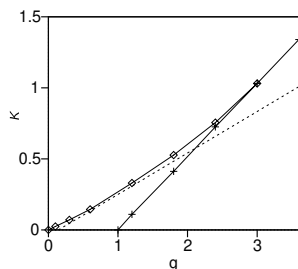


FIG. 3. In the parameter plane of the inter-component repulsion coefficient (g) and linear-mixing coefficient (κ), the outer and inner immiscibilities take place at $\kappa < \kappa_c(g)$, i.e., beneath the chains of crosses and squares, respectively. The solid line with crosses is given by Eq. (50) with density $n = 1$. The two critical lines merge at $g \geq 3$, where there is no difference between the outer and inner immiscibility. The dashed line is the VA prediction for the boundary of the inner immiscibility, as given by Eq. (55) with $n = 1$.

Furthermore, the immiscibility may occur in the DS core even in the case of $g \leq 1$, when the SSB (immiscibility)

does not take place for the CW states even in the absence of the linear coupling. Examples are displayed in Figs. 2(a) and (b), for $g = 1.0$, $\kappa = 0.1$, $k = -0.925$ and $g = 0.1$, $\kappa = 0.006$, $k = -0.573$, respectively (note the similarity of the DS profiles with the inner immiscibility in Figs. 1(b) and 2(a)). Figure 2(c) summarizes these results by plotting $\Delta \equiv |u(x=0) - v(x=0)|$ vs. κ at $g = 0.1$ and 0.6 . The inner immiscibility in the DS core takes place, accordingly, at $\kappa < 0.025$ for $g = 0.1$ and $\kappa < 0.145$ for $g = 0.6$. Naturally, the largest value of κ admitting the inner immiscibility increases with the increase of g , as the linear coupling (κ) and nonlinear repulsion (g) of the two components are competing factors. It is natural too that no inner immiscibility is observed for $g = 0$.

The numerically found boundaries of the outer and inner immiscibility in the parameter plane of (g, κ) are plotted in Fig. 3 by the dashed and solid lines, respectively. With fixed $N = L = 100$, both boundaries correspond to the CW background with density $n = N/L = 1$. The substitution of this value in Eq. (20) yields the threshold (critical) value of the linear coupling which determines the onset of SSB in the CW state, i.e., the boundary of the outer immiscibility,

$$\kappa_c = (g - 1)n/2, \quad (50)$$

which exactly corresponds to the dashed line in Fig. 3. The two boundaries merge in Fig. 3 at $g = 3$, where the DS is given by the exact solution (39), there being no distinction between the outer and inner immiscibility in the DS states at $g \geq 3$.

The stability of all DSs featuring the inner-only and outer immiscibilities, including the exact solution given by Eq. (39) for $g = 3$, has been verified by simulations of their perturbed evolution. On the other hand, it was found that all exact symmetry-breaking DS solutions (45), attached to the PT potential, are unstable, for $g < 3$ and $g > 3$ alike (not shown here in detail). In particular, in the case of $g > 3$, when the PT potential (44) is attractive, the instability is explained by the general fact that DSs are *repelled* by attractive local potentials (see, e.g., Ref. [41]). In the case of $g < 3$, the effective *attraction* of the zero-crossing points (47) to the local *repulsive* potential also implies an instability. It is relevant to mention that, along with the DSs, the PT potential also admits exact solutions of the DW type. Additional analysis (not presented here) demonstrates that the DW pinned to the PT potential is stable at $g < 3$ and unstable $g > 3$ (a similar result for the DWs was recently obtained in Ref. [42]).

B. The variational approximation (VA) for the DS with the inner immiscibility

While the onset of the outer immiscibility in the DSs is readily explained by the exact solution (17) for the symmetry-breaking CW background states, the inner immiscibility, which is exhibited, in Figs. 1(b) and 2(a), by the DS cores supported by the symmetric CW background, can be explained, in a crude analytical approximation, by means of VA (see Ref. [43] for a review). To this end, we use the Lagrangian of the system of Eqs. (5) and (6), defined on the circumference of perimeter L :

$$\mathcal{L} = \int_{-L/2}^{+L/2} \left\{ \frac{1}{4} \left[\left(\frac{\partial u}{\partial x} \right)^2 + \left(\frac{\partial v}{\partial x} \right)^2 \right] + \frac{k}{2} (u^2 + v^2) + \frac{1}{4} (u^4 + v^4) + \frac{g}{2} u^2 v^2 - \kappa uv \right\} dx. \quad (51)$$

A natural ansatz for a DS with the u and v components separated (demixed) inside the core and merged (mixed) in the CW background is adopted as

$$u = U \left[\tanh(\xi x) + \frac{a}{\cosh(\xi x)} \right], \quad v = U \left[\tanh(\xi x) - \frac{a}{\cosh(\xi x)} \right], \quad (52)$$

with coefficients U and ξ taken as per the symmetric DS solution (34), with density n defined as per Eq. (14):

$$U = \sqrt{\frac{\kappa - k}{1 + g}} \equiv \sqrt{\frac{n}{2}}, \quad \xi = \sqrt{\kappa - k}, \quad (53)$$

while a is a free variational parameter. The substitution of ansatz (52) in Lagrangian (51) yields

$$\begin{aligned} \mathcal{L} = & \frac{U^2}{3\xi} (\xi^2 + 6U^2 + 6k + 6\kappa - 2gU^2 a^2) + \frac{2}{3\xi} (1 + g) U^4 a^4 \\ & + L \left[(k - \kappa) \frac{n}{2} + (g + 1) \frac{n^2}{8} \right], \end{aligned} \quad (54)$$

where the last (bulk) term, $\sim L$, is an a -independent contribution from the CW background. Further, the chemical potential $-k$ in Eq. (54) is replaced by expression $-k = (1 + g)n/2 - \kappa$, according to Eq. (53). Then, the variational

(Euler-Lagrange) equation is produced by Lagrangian (54) as $\partial\mathcal{L}/\partial(a^2) = 0$. After a simple algebra, the latter equation predicts the following critical (threshold) value of the linear coupling at which the inner immiscibility commences:

$$\kappa_c = (7g - 1)n/24, \quad (55)$$

cf. its counterpart (50), which is the exact result for the CW states [negative value produced by Eq. (55) at $g < 1/7$ is an artifact of the VA].

V. VORTEX STATES WITH THE INTER-COMPONENT SHIFT IN THE TWO-DIMENSIONAL BINARY BEC

The system of coupled GP equations for the 2D binary BECs is written as a straightforward extension of the 1D system of Eqs. (2) and (3):

$$i\phi_t = -\kappa\psi - \frac{1}{2}(\phi_{xx} + \phi_{yy}) + (|\phi|^2 + g|\psi|^2)\phi, \quad (56)$$

$$i\psi_t = -\kappa\phi - \frac{1}{2}(\psi_{xx} + \psi_{yy}) + (|\psi|^2 + g|\phi|^2)\psi. \quad (57)$$

Stationary 2D states are looked for as

$$\phi(x, y, t) = e^{ikt}u(x, y), \quad \psi(x, y, t) = e^{ikt}v(x, y), \quad (58)$$

with complex functions $u(x, y)$ and $v(x, y)$ satisfying equations

$$-ku + \kappa v = -\frac{1}{2}\left(\frac{d^2}{dx^2} + \frac{d^2}{dy^2}\right)u + (|u|^2 + g|v|^2)u, \quad (59)$$

$$-kv + \kappa u = -\frac{1}{2}\left(\frac{d^2}{dx^2} + \frac{d^2}{dy^2}\right)v + (|v|^2 + g|u|^2)v. \quad (60)$$

Vortex states, supported by the CW background, are 2D counterparts of the 1D DSs. In terms of phases $\alpha(x, y)$ and $\beta(x, y)$ of the complex fields $u(x, y)$ and $v(x, y)$ [cf. Eq. (25)], integer vorticity S (alias the winding number, or topological charge) is defined as usual [44]: $S = \Delta\alpha/(2\pi) = \Delta\beta/(2\pi)$, where $\Delta\alpha$ and $\Delta\beta$ are phase circulations along trajectories enclosing the vortex core. The 2D states with $S = 0$ amount to the CW solution.

The systems of Eqs. (56), (57) and (59), (60) was solved in the 2D domain $-L/2 < x, y < +L/2$, with periodic boundary conditions imposed in both directions. Accordingly, a vortex-antivortex pair is created under the periodic boundary condition, while here we display the vortex centered at the origin. The solutions are characterized by the 2D norm,

$$N_{2D} = \int_{-L/2}^{+L/2} dx \int_{-L/2}^{+L/2} dy \left[|\phi(x, y)|^2 + |\psi(x, y)|^2 \right]. \quad (61)$$

The symmetry-breaking CW states in the 2D case are the same as given by Eq. (17), and are equally stable. Stable vortex modes supported by such background states demonstrate a specific 2D feature in the form of a shift between their u and v components, as shown in Fig. 4, for $S = 1$ and parameters

$$g = 2, \kappa = 0.45, k = -1.1, N = 400, L = 20 \quad (62)$$

[note that these parameters satisfy condition (19) which maintains the asymmetric CW states]. The shift between the two components of the vortex mode is a direct counterpart of the separation between the components in the 1D DSs maintained by the asymmetric background. In the example displayed in Fig. 4, the vortical cores in the coupled components are mutually shifted in the x direction, thus breaking the cores' isotropy. The direction of the shift may be arbitrary, selected by initial conditions.

The consideration of the 1D system presented above has produced, in addition to the DSs with the outer immiscibility, supported by the symmetry-breaking CW background [see Fig. 1(a)], also DS modes featuring the inner immiscibility in their cores, while the CW background remains symmetric [see Fig. 1(b) and 2(a); recall that such modes populate the area between the solid and dashed lines in Fig. 3]. Similarly, the 2D system is capable to produce

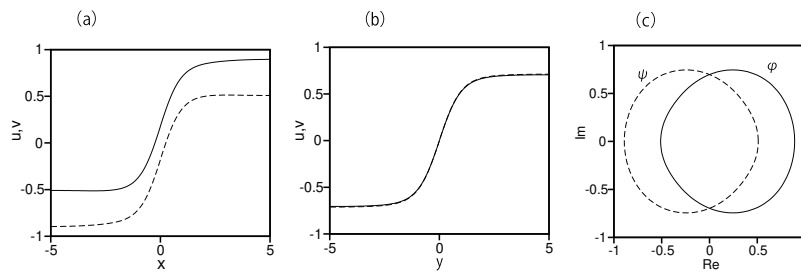


FIG. 4. (a) The cross-sections of $\text{Re}(u(x,y))$ and $\text{Re}(v(x,y))$ (solid and dashed lines, respectively) in the numerically found stable vortex state with $S = 1$, maintained by the asymmetric CW background, along $y = 0$. (b) The cross sections of $\text{Im}(u(x,y))$ and $\text{Im}(v(x,y))$ (solid and dashed lines, respectively) along $x = 0$. (c) $(\text{Re } \phi, \text{Im } \phi)$ and $(\text{Re } \psi, \text{Im } \psi)$ (solid and dashed loops, respectively) along the circumference of radius $r = 4$. The parameters are given by Eq. (62).

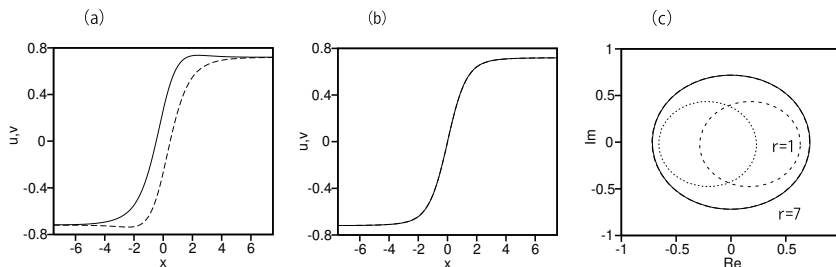


FIG. 5. Panels (a) and (b) display the same as in Figs. 4(a,b), but for parameters (63). Panel (c) is similar to Fig. 5(c), with the difference that the parameters are taken as per Eqs. (63), while $(\text{Re } \phi, \text{Im } \phi)$ and $(\text{Re } \psi, \text{Im } \psi)$ are plotted along two circumferences, with radii $r = 1$ and 7 .

stable vortices maintained by the symmetric CW background, with the inner shift between their vortical cores. An example is displayed in Fig. 5(a), for $S = 1$ and parameters

$$g = 0.8, \kappa = 0.08, k = -0.865, N = 900, L = 30. \quad (63)$$

The systematic analysis demonstrates that, for $g = 0.8$ and $N = 900, L = 30$, i.e., with the background density $n \approx 1$, the shift (splitting) between the vortical cores of the two components persists at $\kappa \leq \kappa_c \approx 0.095$ [in particular, $\kappa = 0.08$ in Eq. (63) satisfies the latter condition]; for comparison, it is relevant to mention that the critical value of κ for supporting the inner immiscibility in the 1D DS at $g = 0.8$ and $n = 1$ is much larger, $\kappa_c \approx 0.205$. In particular, Fig. 5(c) clearly demonstrates the inner character of the shift: the splitting between the cores is strong along the circumference of radius $r = 1$, but is absent for $r = 7$.

Systematically collected numerical results verify stability of the $S = 1$ vortices with the global or inner shift between the cores of their components. On the other hand, the well-known results for the single-component GP/NLS equations [28, 44] suggest that vortices with $S \geq 2$ may be unstable against spontaneous splitting into sets of unitary ones.

VI. CONCLUSION

We have considered a system which models the copropagation of two circular polarizations of light in the self-defocusing optical fiber with the linear mixing of the polarizations, as well as the dynamics of the two-component self-repulsive BEC with the Rabi coupling in 1D and 2D free-space settings alike. A new effect which is demonstrated by the system is the SSB (spontaneous symmetry breaking) in the bimodal CW state in the case when the relative strength of the inter-component repulsion takes values $g > 1$ (which corresponds to the full immiscibility, in the absence of the linear mixing). Exact analytical solutions for stable symmetry-breaking CW states are obtained. Further, we have found the exact solution for stable 1D DS (dark soliton) supported by the asymmetric (partly immiscible) CW background in the case of $g = 3$. For $g \neq 3$, generic symmetry-breaking DSs are found in the numerical form. The full stability of these modes is established by means of systematic simulations of their perturbed evolution. Furthermore, a parameter region is identified in which the symmetric (fully miscible) CW background supports stable DSs with the

partial immiscibility of the two components, in its core. The 2D system gives rise to stable vortex modes with the shift (splitting) between the two components, which breaks the vortex' isotropy. These modes include ones in which the global shift is imposed by the asymmetric CW background, as well as modes with the symmetric background, in which the local shift takes place between the vortical cores of the two components.

As an extension of the analysis, it may be interesting to consider interactions between the symmetry-breaking DSs in 1D, and interactions between the bimodal vortices with shifted components in 2D. It is also relevant to extend the analysis to dissipative systems, modeled by coupled complex Ginzburg-Landau equation [25]. In particular, experimental observation of polarization SSB in dissipative solitons in a fiber laser was very recently reported in Ref. [26].

ACKNOWLEDGMENT

We appreciate valuable discussions with Eyal Buks. The work of B.A.M. was supported, in part, by the Israel Science Foundation through grant No. 1695/22.

-
- [1] *Spontaneous Symmetry Breaking, Self-Trapping, and Josephson Oscillations* (B.A. Malomed, Editor, Springer, Berlin, 2013).
 - [2] S. M. Jensen, The nonlinear coherent coupler, *IEEE J. Quantum Electron* **18**, 1580–1583 (1982).
 - [3] A. A. Maier, Optical transistors and bistable devices utilizing nonlinear transmission of light in systems with unidirectional coupled waves, *Sov. J. Quantum Electron* **12**, 1490–1494 (1982).
 - [4] M. Albiez, R. Gati, J. Fölling, S. Hunsmann, M. Cristiani, and M. K. Oberthaler, Direct Observation of Tunneling and Nonlinear Self-Trapping in a Single Bosonic Josephson Junction, *Phys. Rev. Lett.* **95**, 010402 (2005).
 - [5] M. Trippenbach, E. Infeld, J. Gocalek, M. Matuszewski, M. Oberthaler, and B. A. Malomed, Spontaneous symmetry breaking of gap solitons and phase transitions in double-well traps, *Phys. Rev. A* **78**, 013603 (2008).
 - [6] H. Sakaguchi and B. A. Malomed, Symmetry breaking of solitons in two-component Gross-Pitaevskii equations, *Phys. Rev. E* **83**, 036608 (2011).
 - [7] B. Abdo, E. Arbel-Segev, O. Shtempluck, and E. Buks, Observation of bifurcations and hysteresis in nonlinear NbN superconducting microwave resonators, *IEEE Transactions on Applied Superconductivity* **16**, 1976–1987 (2006).
 - [8] A. W. Snyder, D. J. Mitchell, L. Poladian, D. R. Rowland, and Y. Chen, Physics of nonlinear fiber couplers, *J. Opt. Soc. Am. B* **8**, 2101–2118 (1991).
 - [9] G. P. Agrawal, *Nonlinear Fiber Optics* (Academic Press, Amsterdam, 2013).
 - [10] E. M. Wright, G. I. Stegeman, and S. Wabnitz, Solitary-wave decay and symmetry-breaking instabilities in two-mode fibers, *Phys. Rev. A* **40**, 4455–4466 (1989).
 - [11] F. K. Abdullaev, R. M. Abrarov, and S. A. Darmanyan, Dynamics of solitons in coupled optical fibers. *Opt. Lett.* **14**, 131–133 (1989).
 - [12] C. Paré and M. Flórjańczyk, Approximate model of soliton dynamics in all-optical couplers, *Phys. Rev. A* **41**, 6287–6295 (1990).
 - [13] A. I. Maimistov, Propagation of a light pulse in nonlinear tunnel-coupled optical waveguides, *Kvant. Elektron.* **18**, 758–761 [*Sov. J. Quantum Electron.* **21**, 687–690 (1991)].
 - [14] M. Romagnoli, S. Trillo, and S. Wabnitz, Soliton switching in nonlinear couplers. *Opt. Quantum Electron.* **24**, S1237–S1267 (1992).
 - [15] N. Akhmediev and A. Ankiewicz, Novel soliton states and bifurcation phenomena in nonlinear fiber couplers, *Phys. Rev. Lett.* **70**, 2395–2398 (1993).
 - [16] J. M. Soto-Crespo and N. Akhmediev, Stability of the soliton states in a nonlinear fiber coupler, *Phys. Rev. E* **48**, 4710–4715 (1993).
 - [17] K. S. Chiang, Intermodal dispersion in two-core optical fibers, *Opt. Lett.* **20**, 997–999 (1995).
 - [18] P. L. Chu, Yu. S. Kivshar, B. A. Malomed, G. D. Peng, and M. L. Quiroga-Teixeiro, Soliton controlling, switching, and splitting in fused nonlinear couplers, *J. Opt. Soc. Am. B* **12**, 898 (1995).
 - [19] B. A. Malomed, I. M. Skinner, P. L. Chu, and G. D. Peng, Symmetric and asymmetric solitons in twin-core nonlinear optical fibers, *Phys. Rev. E* **53**, 4084–4081 (1996).
 - [20] N. F. Smyth and A. L. Worthy, Dispersive radiation and nonlinear twin-core fibers, *J. Opt. Soc. Am. B* **14**, 2610–2617 (1997).
 - [21] V. H. Nguyen, L. X. T. Tai, I. Bugar, M. Longobucco, R. Buczynski, B. A. Malomed, and M. Trippenbach, Reversible ultrafast soliton switching in dual-core highly nonlinear optical fibers, *Opt. Lett.* **45**, 5221–5224 (2020).
 - [22] H. Sakaguchi and B. A. Malomed, Symmetry breaking in a two-component system with repulsive interactions and linear coupling, *Comm. Nonlin. Sci. Num. Sim.* **92**, 105496 (2021).
 - [23] S. Flügge, *Practical Quantum Mechanics* (Springer-Verlag, Berlin, 1998).

- [24] B. A. Malomed, A variety of dynamical settings in dual-core nonlinear fibers, In: *Handbook of Optical Fibers*, Vol. 1, pp. 421-474 (G.-D. Peng, Editor: Springer, Singapore, 2019).
- [25] A. Sigler and B. A. Malomed, Solitary pulses in linearly coupled cubic-quintic Ginzburg-Landau equations, *Physica D* **212**, 305–316 (2005).
- [26] Y. Yang, X. Chen, W. Lin, X. Hu, H. Xu, Y. Ma, Z. Liang, L. Ling, Z. Xiong, Y. Guo, T. Liu, X. Wei and Z. Yang, Polarization Symmetry Breaking of GHz Dissipative Soliton, *Phys. Rev. Lett.* **134**, 213803 (2025).
- [27] L. P. Pitaevskii and S. Stringari, *Bose-Einstein Condensation* (Oxford University Press, Oxford, 2003).
- [28] G. A. Swartzlander and C. T. Law, Optical vortex solitons observed in Kerr nonlinear media, *Phys. Rev. Lett.* **69**, 2503-2506 (1992).
- [29] Y. S. Kivshar and B. Luther-Davies, Dark optical solitons: physics and applications. *Phys. Rep.* **298**, 61-197 (1998).
- [30] V. P. Mineev, The theory of the solution of two near-ideal Bose gases, *Zh. Eksp. Teor. Fiz.* **67**, 263-272 (1974) [English translation: *Sov. Phys. – JETP* **40**, 132-136 (1974)].
- [31] G. P. Agrawal, Modulational instability induced by cross-phase modulation, *Phys. Rev. Lett.* **59**, 880-883 (1987).
- [32] D. E. Pelinovsky, *Localization in Periodic Potentials: From Schrödinger Operators to the Gross-Pitaevskii Equation* (Cambridge University Press, Cambridge (UK), 2011).
- [33] R. J. Ballagh, K. Burnett, and T. F. Scott, Theory of an Output Coupler for Bose-Einstein Condensed Atoms, *Phys. Rev. Lett.* **78**, 1607-1611 (1997).
- [34] S. D. Jenkins and T. A. B. Kennedy, Dynamic stability of dressed condensate mixtures, *Phys. Rev. A* **68**, 053607 (2003).
- [35] B. A. Malomed, A. A. Nepomnyashchy, and M. I. Tribelsky, Domain boundaries in convection patterns, *Phys. Rev. A* **42**, 7244-7263 (1990).
- [36] B. A. Malomed, New findings for the old problem: Exact solutions for domain walls in coupled real Ginzburg-Landau equations, *Phys. Lett. A* **422**, 127802 (2022).
- [37] K. E. Strecker, G. B. Partridge, A. G. Truscott, and R. G. Hulet, Bright matter wave solitons in Bose-Einstein condensates, *New J. Phys.* **5**, 73 (2003).
- [38] A. L. Marchant, T. P. Billam, T. P. Wiles, M. M. H. Yu, S. A. Gardiner, and S. L. Cornish, Controlled formation and reflection of a bright solitary matter-wave, *Nature Comm.* **4**, 1865 (2013).
- [39] M. L. Chiofalo, S. Succi, and M. P. Tosi, Ground state of trapped interacting Bose-Einstein condensates by an explicit imaginary-time algorithm, *Phys. Rev. E* **62**, 7438-7444 (2000).
- [40] W. Z. Bao and Q. Du, Computing the ground state solution of Bose-Einstein condensates by a normalized gradient flow, *SIAM J. Sci. Comp.* **25**, 1674-1697 (2004).
- [41] M. Ma, R. Carretero-González, P. G. Kevrekidis, D. J. Frantzeskakis, and B. A. Malomed, Controlling the transverse instability of dark solitons and nucleation of vortices by a potential barrier. *Phys. Rev. A* **82**, 023621 (2010).
- [42] B. B. Baizakov, B. A. Malomed, and M. Salerno, Nonlinear management of the miscibility-immiscibility transition in binary Bose-Einstein condensates, *Phys. Rev. E*, in press; arXiv:2507.13683.
- [43] B. A. Malomed, Variational methods in nonlinear fiber optics and related fields. *Progr. Optics* **43**, 71-193 (2002).
- [44] A. L. Fetter, Rotating trapped Bose-Einstein condensates, *Rev. Mod. Phys.* **81**, 647-691 (2009).